

Four new PLanetesimals Around TYpical and Pre-main seqUence Stars (PLATYPUS) Debris Discs at 8.8mm

Brodie J. Norfolk^{1*}, Sarah T. Maddison¹, Jonathan P. Marshall^{2,3}, Grant M. Kennedy^{4,5}, Gaspard Duchêne^{6,7}, David J. Wilner⁸, Christophe Pinte^{9,10}, Attila Moór^{11,12}, Brenda Matthews^{13,14}, Péter Ábrahám^{11,12}, Ágnes Kóspál^{11,12,15}, Nienke van der Marel^{13,14}

¹Centre for Astrophysics and Supercomputing (CAS), Swinburne University of Technology, Hawthorn, Victoria 3122, Australia

²Academia Sinica, Institute of Astronomy and Astrophysics, 11F Astronomy-Mathematics Building, NTU/AS campus, No. 1, Section 4, Roosevelt Rd., Taipei 10617, Taiwan

³Centre for Astrophysics, University of Southern Queensland, Toowoomba, QLD 4350, Australia

⁴Department of Physics, University of Warwick, Gibbet Hill Road, Coventry, CV4 7AL, UK

⁵Centre for Exoplanets and Habitability, University of Warwick, Gibbet Hill Road, Coventry CV4 7AL, UK

⁶Astronomy Department, University of California, Berkeley, CA 94720, USA

⁷Université Grenoble Alpes / CNRS, Institut de Planétologie et d'Astrophysique de Grenoble, 38000 Grenoble, France

⁸Harvard-Smithsonian Center for Astrophysics, 60 Garden Street, Cambridge, MA 02138, USA

⁹Monash Centre for Astrophysics (MoCA) and School of Physics and Astronomy, Monash University, Clayton Vic 3800, Australia

¹⁰Univ. Grenoble Alpes, CNRS, IPAG, F-38000 Grenoble, France

¹¹Konkoly Observatory, Research Centre for Astronomy and Earth Sciences, Eötvös Loránd Research Network (ELKH),

H-1121 Budapest, Konkoly-Thege Miklós út 15–17, Hungary

¹²ELTE Eötvös Loránd University, Institute of Physics, Pázmány Péter sétány 1/A, 1117 Budapest, Hungary

¹³Department of Physics & Astronomy, University of Victoria, Victoria, BC V8P 5C2

¹⁴Herzberg Astronomy & Astrophysics Programs, National Research Council of Canada, 5071 West Saanich Road, Victoria BC V9E 2E7, Canada

¹⁵Max Planck Institute for Astronomy, Königstuhl 17, 69117 Heidelberg, Germany

Last updated: March 2021

ABSTRACT

Millimetre continuum observations of debris discs can provide insights into the physical and dynamical properties of the unseen planetesimals that these discs host. The material properties and collisional models of planetesimals leave their signature on the grain size distribution, which can be traced through the millimetre spectral index. We present 8.8 mm observations of the debris discs HD 48370, CPD-72 2713, HD 131488, and HD 32297 using the Australian Telescope Compact Array (ATCA) as part of the PLanetesimals Around TYpical Pre-main seqUence Stars (PLATYPUS) survey. We detect all four targets with a characteristic beam size of 5'' and derive a grain size distribution parameter that is consistent with collisional cascade models and theoretical predictions for parent planetesimal bodies where binding is dominated by self-gravity. We combine our sample with 19 other millimetre-wavelength detected debris discs from the literature and calculate a weighted mean grain size power law index which is close to analytical predictions for a classical steady state collisional cascade model. We suggest the possibility of two distributions of q in our debris disc sample; a broad distribution (where $q \sim 3.2 - 3.7$) for "typical" debris discs (gas-poor/non-detection), and a narrow distribution (where $q < 3.2$) for bright gas-rich discs. Or alternatively, we suggest that there exists an observational bias between the grain size distribution parameter and absolute flux which may be attributed to the detection rates of faint debris discs at \sim cm wavelengths.

Key words: circumstellar matter – planetary systems – planets and satellites: dynamical evolution and stability – techniques: interferometric.

1 INTRODUCTION

Debris discs are the final stage of protoplanetary disc evolution (Williams & Cieza 2011; Wyatt et al. 2015). The majority of pri-

* Contact e-mail: bnorfolk@swin.edu.au

mordial gas has either accreted onto the star/companions or been blown away by photoevaporative winds, and the remaining dust is replenished through ongoing collisions between dust-producing planetesimals, i.e. asteroids and comets (Wyatt 2008; Matthews et al. 2014).

Collisions in the disc are driven by planetesimal stirring that is triggered by either the interaction with smaller bodies that excite the belt (Kenyon & Bromley 2002, 2008; Krivov & Booth 2018), or by the dynamical influence of fully formed planets (Mustill & Wyatt 2009). The size distribution of the grains produced by these collisions provides insight into the different physical and dynamical properties of the invisible parent planetesimals. The original collisional cascade model was formulated by Dohnanyi (1969), who used a power-law grain size distribution $dn(a) \propto a^{-q} da$, and determined $q = 3.5$ for grains with constant tensile strength and velocity dispersion. More recently, this standard model has been improved upon to include grain-size dependant tensile strengths (Pan & Sari 2005) and velocity distributions (Gáspár et al. 2012a; Pan & Schlichting 2012) which result in a range of the grain size distribution exponent q between 3 and 4. This theoretically estimated range of q is supported by a number of millimetre wavelength observations (Ricci et al. 2012, 2015b; MacGregor et al. 2016; Marshall et al. 2017; Wilner et al. 2018; Moór et al. 2020). To date, numerical modelling of observations has constrained the parameter to $3.2 < q < 3.8$ for various grain materials (Hughes et al. 2018; Löhne 2020).

The underlying properties of parent planetesimals remains unknown. Observing multiple discs across a range of spectral types and ages can help address this. To further constrain the material properties of dusty debris discs, multi-wavelength observations in the millimetre regime are required to determine the millimetre spectral index, α_{mm} (Beckwith et al. 1990; Gáspár et al. 2012a). α_{mm} is a function of the dust emissivity and can be used to constrain the collisional state of the disc (Krivov 2010; Ricci et al. 2012, 2015b). Despite their faint emission, observing at longer wavelengths (~ 1 cm) provides a better constraint on the mm spectral index (a long lever arm) and is effectively in the Rayleigh-Jeans regime for typical disk temperatures. Here, we present new results from PLATYPUS, an ongoing survey of debris discs at 8.8 mm with the Australian Telescope Compact Array (ATCA) (Ricci et al. 2015b; Marshall et al. 2017). The targets in this work are four relatively young debris disc host stars spanning a broad range of stellar luminosities that, including sources from the previously largest disc comparison survey (Löhne 2020), increases the number of systems with measured values to 22.

2 THE SAMPLE

The PLATYPUS sample are selected to have (1) declinations below 20 degrees in order to be observable with the ATCA array, (2) complementary ALMA observations at 1.3 mm, and (3) are relatively compact to maximize surface brightness sensitivity. In this work we add an additional four debris discs not previously observed at long wavelengths that span a range of spectral types and are comparatively young (50 Myr or less). We summarise the relevant stellar properties of the four sources in Table 1.

2.1 HD 48370

HD 48370 is a G8 V star (Torres et al. 2008) at a distance of 36.07 ± 0.07 pc (Gaia Collaboration et al. 2018) and has an estimated age of ~ 20 –50 Myr (Torres et al. 2008). A peak radius for the disc

Table 1. Stellar properties of our four new PLATYPUS sources.

source	RA	dec	distance (pc)	SpType	age (Myr)
HD 48370	06:43:01	-02:53:19	36.07 ± 0.07	G8	20-50
CPD-72 2713	22:42:48	-71:42:21	36.66 ± 0.03	K7-M0	24
HD 131488	14:55:08	-41:07:13	155 ± 2	A1	15
HD 32297	05:02:27	+07:27:39	133 ± 1	A5-A6	15-45

to be at ~ 90 au using spatially resolved *Herschel* images (Moór et al. 2016; Marshall et al. 2021). Using archival 1.3 mm ALMA observations (Project ID: 2016.2.00200S) of HD 48370, we fit a simple Gaussian to the observatory-calibrated visibilities and derive an integrated flux of 5.0 ± 0.5 mJy.

2.2 CPD-72 2713

CPD-72 2713 (CPD-72) is a late-type star with a derived spectral type of K7–M0 (Torres et al. 2006; Pecaú & Mamajek 2013; Gaidos et al. 2014). It resides at a distance of 36.66 ± 0.03 pc (Gaia Collaboration et al. 2018) and is a member of the ≈ 24 Myr old β Pic moving group (Torres et al. 2006; Bell et al. 2015; Lee & Song 2018; Gagné et al. 2018). With new 1.33 mm ALMA observations, Moór et al. (2020) estimates the outer radius of the cold debris disc surrounding the host star to be 140 ± 14 au.

2.3 HD 131488

HD 131488 is an A2 type star (Melis et al. 2013) residing at a distance of 155 ± 2 pc (Gaia Collaboration et al. 2018) and is ~ 15 Myr old (Mamajek et al. 2002; Pecaú et al. 2012). It is a member of the Upper Centaurus Lupus moving group in the Sco-Cen association (Rizzuto et al. 2011). By analysing spatially resolved ALMA continuum observations, Moór et al. (2017) derived a disc radius of $\sim 0''.57$ (~ 88 au). They also found that the disc harbours a substantial amount of CO gas ($\sim 0.1 M_{\oplus}$, considering the Gaia DR2 based distance of the object).

2.4 HD 32297

HD 32297 is an A5 V or A6 V type star (Debes et al. 2009) at a distance of 133 ± 1 pc (Gaia Collaboration et al. 2018). Kalas (2005) estimates an age less than 30 Myr, whereas Esposito et al. (2020) derived a range of 15–45 Myr. MacGregor et al. (2018) fit the visibilities of high-resolution 1.3 mm ALMA observations and derive the inner edge of the planetesimal belt to be 76 ± 8 au and the inner edge of the disc halo to be 122 ± 3 au, in agreement with previous Keck/NIRC2 imaging (Currie et al. 2012). They also constrain the outer edge of the halo to 440 ± 32 au, closely matching estimates from *HST* images (Schneider et al. 2005). Duchêne et al. (2020) found the disk to be extremely symmetric in scattered light, with disc morphology in reasonable agreement with the ALMA results from MacGregor et al. (2018). HD 32297 is considered a CO-rich disc (Greaves et al. 2016) with a mass of $7.4 \times 10^{-2} M_{\oplus}$. This is the second most massive after HD131488, see MacGregor et al. (2018) and Moór et al. (2019), and is one of four CO-rich debris discs around ~ 30 –40 Myr A-type stars found to date, joining HD 21997 (Moór et al. 2011) and 49 Ceti (Zuckerman & Song 2012).

3 ATCA OBSERVATIONS AND DATA REDUCTION

We used the ATCA radio telescope to conduct our survey at 34 GHz (project code C2694, PI: Maddison). The Compact Array Broadband Backend (CABB, Wilson et al. 2011) provides observations with two bands that contain 2048×1 MHz channels, which we centred at 33 GHz and 35 GHz. Observations were conducted in the hybrid H214 array configuration with antenna 6 flagged due to the increased phase noise on long baselines. This sets an effective baseline range from 92 m to 247 m. The synthesised beam for each observation is detailed in Table 2. The weather during the observations varied for each science target, and the seeing monitor RMS path length noise for each observation is summarised in Table 2.

The science targets were observed with a repeated sequence of 10 min on-source integration and 2 min integration of the gain/phase calibrator. The bandpass and flux calibrators were observed for ~ 15 min and pointing checks were made on the phase calibrator every ~ 60 –90 min. All observational and calibration details are summarised in Table 2.

The data was processed using the software package MIRIAD (Sault et al. 1995) and followed the standard procedure which involved: correcting for the frequency-dependent gain using the MIRIAD task *mfcal*; then using the flux density of the ATCA primary flux calibrator, 1937-638, to re-scale the visibilities measured by the correlator using the miriad task *mfcal* with the option *nopassol* set; and correcting for the gain of the system’s time variable properties due to changing conditions using the MIRIAD task *gpcal*. To reduce the noise in our data while maintaining as complete an observational track as possible, we flagged all data with a seeing monitor RMS path length noise above $400 \mu\text{m}$ using *uvflag*, and calibrator amplitude readings that deviated more than 10% from the mean flux using *blflag*. Any unusual spikes seen in the channel vs. amplitude or the channel vs. phase plots were also flagged using *uvflag*. We adopt a 10% uncertainty on the absolute flux scale for our ATCA observations that is typical at these wavelengths (Ubach et al. 2012), and in agreement with the variations we observe of the gain calibrator flux.

After calibrating the data, images at 34 GHz were produced using robust weighting of 2 to achieve natural weighting and retain maximum detectable flux. The dirty images were cleaned to 5σ (5 times the RMS noise level) using the *clean* task and the beam was restored using the *restor* task. The resulting images for our four sources are presented in Figure 1. HD 48370, HD 131488, and HD 32297 exhibit a north-south alignment of residual emission peaks. This is an artefact from clean due to poorly sampling in *uv*-space. Given the marginal detection ($\sim 3\sigma$) and beam size with respect to the 3σ contours, the discs are consistent with being unresolved and the flux density is calculated using the *imfit* task (Table 2) with the *source* parameter set to "point". This fits a Gaussian with a width equal to the point-spread-function. We are unable to confirm the presence of stellar emission in our detections. To check for other forms of long wavelength emission in our sources, either resolved observations or temporal monitoring is required (Ubach et al. 2017). However, there was a lack of strong, short (< 15 min) flares that would present as obvious deviations in the amplitude vs. time relation for each target.

4 RESULTS

4.1 Spectral Energy Distributions

We combine our four newly acquired ATCA 8.8 mm flux measurements with photometry from the literature to derive flux density distributions. The photometry comes from a wide variety of sources, including Stömgren *uvby* (Pauzen 2015), Gaia (Gaia Collaboration et al. 2018), 2MASS (Cutri et al. 2012), WISE (Wright et al. 2010), Herschel PACS (Sibthorpe et al. 2018, using our own PSF photometry), and various (sub-)mm papers (see Table 3 for references). We then simultaneously fit stellar and disc components as described by Yelverton et al. (2019); we use PHOENIX models (Allard et al. 2012) for the stellar photosphere component, and a ‘modified’ blackbody function for the disc. The modified blackbody is simply a normal Planck function $B_\nu(T)$ where the emission is blackbody-like and is multiplied by an additional factor $(\lambda_0/\lambda)^{-\beta}$ beyond a fitted ‘break’ wavelength λ_0 where the slope becomes steeper. The spectral slope at long wavelengths (i.e. beyond λ_0) is therefore $2-\beta$. Where a significantly better fit is found, two disc components are used (e.g. Chen et al. 2009; Kennedy & Wyatt 2014), though here we are focused on the parameters of the cooler component which contributes to the sub-mm and mm flux. The best fit models for HD 48370 and CPD-72 suggest a single dust belt is present at 39 K and 45 K respectively, whereas for HD 131488 and HD 32297 warm and cold belts were required at 414 K and 87 K, and 225 K and 82 K, respectively. Our targets have fairly shallow mm-wave slopes, meaning that the fitted values of β are close to zero and λ_0 is essentially unconstrained. As a result, we do not quote the results for λ_0 in this manuscript. We assume a 10% uncertainty on our derived temperatures which is generous, albeit has a minimal effect on q and is contained within the flux errors associated with the spectral mm index.

4.2 Determining the Grain Size Distribution Parameter

We derive the power law index of the dust grain distribution q in an identical fashion to MacGregor et al. (2016). Briefly, this involves calculating the slope of the Planck function, α_{Pl} , for our 8.8 mm fluxes and the next longest wavelength, which for our sample is at 1.3 mm:

$$\alpha_{\text{Pl}} = \left| \frac{\log(B_{\nu_1}/B_{\nu_2})}{\log(\nu_1/\nu_2)} \right| \quad (1)$$

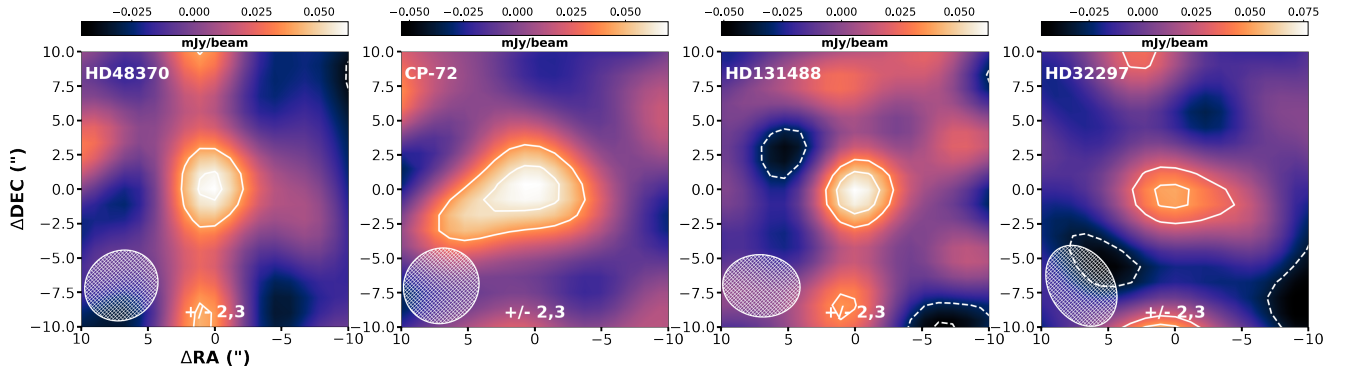
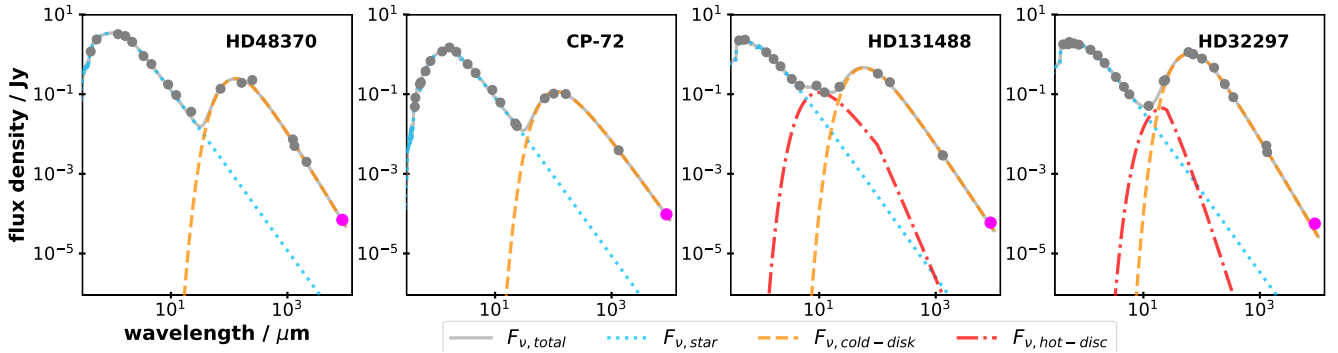
where B_ν is the Planck function at the dust temperature T_d (taken as the fitted temperature of the cool disc component in the SEDs) and $\nu_{1,2}$ are the frequencies of our two longest wavelength observations. The mm spectral index can then be calculated via $\alpha_{\text{mm}} = |\log(F_{\nu_1}/F_{\nu_2})/\log(\nu_1/\nu_2)|$. Assuming both flux measurements are in the Rayleigh-Jeans limit, q is then derived through the relation:

$$q = \frac{\alpha_{\text{mm}} - \alpha_{\text{Pl}}}{\beta_s} + 3 \quad (2)$$

Draine (2006) analytically derives the q - β relation (where q is referred to as p in the manuscript) for grains in protoplanetary discs where β_s is the dust opacity spectral index of small particles. This relationship is valid for values of q in the range of 3–4 which are typical for debris discs. The value of β_s is dependent on the assumed material composition of the dust. β_s can vary from 1.3–2 (Jaeger et al. 1994; Draine 2004), however the variation in β_s is comparable to the uncertainties on q derived from our analysis. We therefore assume that our grains are composed of astronomical silicate where

Table 2. PLATYPUS survey results and observing log.

Source	Flux Density (μJy)	1σ (μJy)	θ_{beam} ($" \times "$)	Date	Obs. Time (min)	Calibrators			Ave. Path Length rms (μm)
						Band-pass	Flux	Gain/Phase	
HD 48370	70.0	10.8	5.61 x 5.01	2019 Mar 01-02	225	1253-055	1934-638	0639-032	255
CPD-72 2713	95.9	16.1	5.74 x 5.40	2019 Mar 02	225	1921-293	1934-638	2229-6910	329
HD 131488	59.5	12.4	5.78 x 4.51	2019 Mar 02	430	1253-055	1934-638	1451-400	111
HD 32297	56.2	16.7	6.37 x 4.73	2019 Mar 01-02	450	0003-066	1934-638	0454+066	282

**Figure 1.** Images of the four debris discs detected in our 8.8-mm ATCA observations. The orientation is north up, east left. The synthesized ATCA beam FWHM extent and orientation for each observations is represented by the shaded ellipse in the bottom left of each panel. Contours are ± 2 and 3σ , with negative contours denoted by dashed lines.**Figure 2.** The spectral energy distributions of our four PLATYPUS debris discs. The magenta marker denotes the ATCA 8.8 mm flux, grey markers represent fluxes from the literature. Circle markers indicate detections above 3σ . The total flux, stellar photosphere, cold disc emission, and hot disc emission are represented by a hard grey line, dotted blue line, dashed orange line, and dash-dot red line respectively.

$\beta_s = 1.8$, consistent with many other debris disc studies (MacGregor et al. 2016; Marshall et al. 2017).

Table 3 presents q values for our four sources calculated using equation 2, along with 18 other debris discs from the literature (see the references in Table 3). Due to an over subtraction during the removal of stellar emission, MacGregor et al. (2016) estimates a lower limit for the disc emission in AU Mic. This results in a counter-intuitive upper limit of the q value.

5 DISCUSSION

Figure 3 shows the distribution of q for 22 debris discs, the largest sub-mm to mm comparison sample to date. We include both the spectral type and age in Figure 3, and find slightly lower corre-

lations between the q value and stellar properties in comparison to findings presented in MacGregor et al. (2016) (for a slightly smaller sample of 15 debris discs). For our sample of 22 debris discs there does not appear to be any correlation between age and the grain size power law. Separating our sample at 50Myr (see Table A1 for target ages), a Kolmogorov-Smirnov (K-S) test estimates a probability of 62% that these two populations are drawn from the same distribution. However, there is a tentative trend with spectral type (slightly weaker than that found by MacGregor et al. (2016)). Separating our sample by A-F stars and G-(K-M) stars, a K-S test estimates a probability of 23% that these two populations are drawn from the same distribution. This suggests that stars with later spectral types may exhibit shallower grain size distributions, as previously seen in Pawellek & Krivov (2015). However, since we increase the percentage of later type stars in our sample com-

Table 3. The complete debris disc sample with sub-mm to mm observations. Our four new PLATYPUS sources with ATCA 8.8 mm fluxes are in bold. $\lambda_{1,\text{mm}}$ and $\lambda_{2,\text{mm}}$ are the wavelengths used to calculate the millimetre spectral slope α_{mm} (flux densities are presented in Table A1). L_{\star} and T_{d} (the dust temperature of the cold component) for our four new sources is derived from the SED modelling. α_{PI} and q are calculated using equations 1 and 2 respectively. This table has been adapted from Löhne (2020).

Source	L_{\star} [L_{\odot}]	Ref.	$\lambda_{1,\text{mm}}$	$\lambda_{2,\text{mm}}$	α_{mm}	Ref.	T_{d} [K]	α_{PI}	q	Ref.
AU Mic	0.1	2	1.3	9.0	< 2.46	2	26	1.87	< 3.33	13
CPD-72 2713	0.19	1	1.3 ^a	8.9	1.95 ± 0.17	1	45	1.94 ± 0.12	3.01 ± 0.09	1
ϵ Eri	0.3	2	1.3	7.0	> 2.39	9	26	1.87	> 3.29	13
HD 61005	0.5	2	1.3	9.0	2.49 ± 0.08	2	30	1.89	3.33 ± 0.04	13
HD 48370	0.77	1	1.3 ^a	8.9	2.26 ± 0.14	1	39	1.93 ± 0.14	3.18 ± 0.08	1
HD 107146	1.0	2	1.25	7.0	2.55 ± 0.11	10	27	1.88	3.37 ± 0.06	13
HD 377	1.0	2	0.87	9.0	> 2.39	2	42	1.92	> 3.26	13
HD 105	1.2	3	0.87	9.0	2.41 ± 0.16	3	33	1.90	3.28 ± 0.09	13
q^1 Eri	1.2	2	0.87	7.0	2.94 ± 0.10	2	33	1.90	3.58 ± 0.06	13
HD 104860	1.4	2	1.3	9.0	3.08 ± 0.23	2	31	1.89	3.66 ± 0.13	13
HD 15115	3.3	2	1.3	9.0	2.75 ± 0.15	2	40	1.92	3.46 ± 0.08	13
HD 181327	3.3	2	1.3	7.0	2.38 ± 0.05	10	42	1.92	3.26 ± 0.03	13
HR 8799	5.4	4	1.3	9.0	2.41 ± 0.17	11	40	1.92	3.27 ± 0.10	11
η Crv	6.6	5	0.85	9.0	2.10 ± 0.07	5,12	38	1.91	3.11 ± 0.04	13
HD 32297	8.2	1	1.3 ^a	8.9	2.11 ± 0.22	1	82	1.97 ± 0.07	3.07 ± 0.12	1
HD 95086	8.6	2	1.3	7.0	2.41 ± 0.12	2	35	1.91	3.27 ± 0.07	13
β Pic	8.7	2	0.87	7.0	2.81 ± 0.10	10	49	1.93	3.49 ± 0.06	13
HD 131835	10.5	6	0.87	9.0	2.17 ± 0.13	12	56	1.94	3.13 ± 0.07	13
HD 131488	12.8	1	1.3 ^a	8.9	2.05 ± 0.17	1	87	1.97 ± 0.06	3.04 ± 0.09	1
Formalhaut	16	2	1.3	7.0	2.70 ± 0.17	2	50	1.93	3.43 ± 0.09	13
49 Ceti	20	2	0.85	9.0	2.76 ± 0.11	2	64	1.95	3.45 ± 0.06	13
HR 4796 A	27	7,8	0.85	9.0	$> 2.73 \pm 0.10$	12	73	1.96	3.43 ± 0.06	13

Notes: ^a λ_1 fluxes are taken from Moór et al. (2020) (CPD-72), this work (HD 48370), MacGregor et al. (2018) (HD32297), and Moór et al. (2017) (HD 131488).

References (1) this work, (2) MacGregor et al. (2016), (3) Marshall et al. (2018), (4) Holland et al. (2017), (5) Marino et al. (2017), (6) Hung et al. (2015a) (7) Gerbaldi et al. (1999), (8) Gaia Collaboration et al. (2016, 2018), (9) MacGregor et al. (2015b), (10) Ricci et al. (2015b), (11) Wilner et al. (2018), (12) Marshall et al. (2017), (13) Löhne (2020).

pared to MacGregor et al. (2016) and our correlation decreases, we suggest that as the later star debris disc sample becomes more populated it's likely that the trend between q and the spectral type will disappear. We also include q -value model predictions from Dohnanyi (1969), Pan & Sari (2005), Pan & Schlichting (2012), Gáspár et al. (2012b), and Schüppler et al. (2015) indicated by the various hatched regions in the plot. The weighted mean q value of the sample, $\langle q \rangle = 3.31 \pm 0.07$, is in close agreement with mean weighted values from previous studies analysing a subset of our sample; $\langle q \rangle = 3.42 \pm 0.07$ (Ricci et al. 2015b), $\langle q \rangle = 3.36 \pm 0.02$ (MacGregor et al. 2016), and $\langle q \rangle = 3.23 \pm 0.04$ (Marshall et al. 2017). These values of q closely align with numerical results from Schüppler et al. (2015) rather than the larger range (3.3–4.6) presented by Pawellek et al. (2014) from far-infrared excesses. The q values derived for our new ATCA observations all fall within the range predicted by Pan & Sari (2005). This suggests that the colliding bodies in these discs have a lower tensile strength and clumping is dominated by self-gravity, resulting in a shallower size distribution. Recently, Löhne (2020) reviewed dust material approximations (β) and compared them with numerical results for a number of materials (Bohren & Huffman 1983; Wolf & Voshchinnikov 2004). They suggest that the inferred grain size distribution indexes from dust material approximations are underestimated. However when comparing a single material, astronomical silicate, their numerical

values for q (seen in their Fig. 14) are contained within our errors in Figure 3.

As expected, the addition of our four new sources to the catalogue of debris discs has little impact on the weighted mean q value. However, all four targets populate the lower range of q values seen to date. In Figure 4, we present the grain size distribution as a function of the interpolated 1 mm flux (Fig. 4a) and the interpolated 1 mm flux scaled to 50 pc (Fig. 4b). Using the `scipy.stats.pearsonr` function, we find a moderate correlation between q and the interpolated flux with a Pearson coefficient of 0.57. After scaling by the distance, this trend is reversed and the correlation is weaker with a Pearson coefficient of -0.22. The absence of discs in the lower-right region of Figure 4a can be attributed to that fact that targets with high fluxes and shallower mm-slopes are defined as protoplanetary discs which are not included in debris disc surveys (e.g. see α_{mm} values presented in Lommen et al. 2007; Norfolk et al. 2021).

For optically thin debris discs, the size distribution index is related to the physics of grain collisions which may be influenced by the presence of gas. Lieman-Sifry et al. (2016) found that CO-rich systems in their sample of 12 resolved debris discs contain grain sizes on lower end of the size distribution. There are eight CO-bearing debris disks in our sample: β Pic (Matrà et al. 2017a), Fomalhaut (Matrà et al. 2017b), η Crv (Marino et al. 2017) and HD 181327 (Marino et al. 2016) contain relatively small amounts

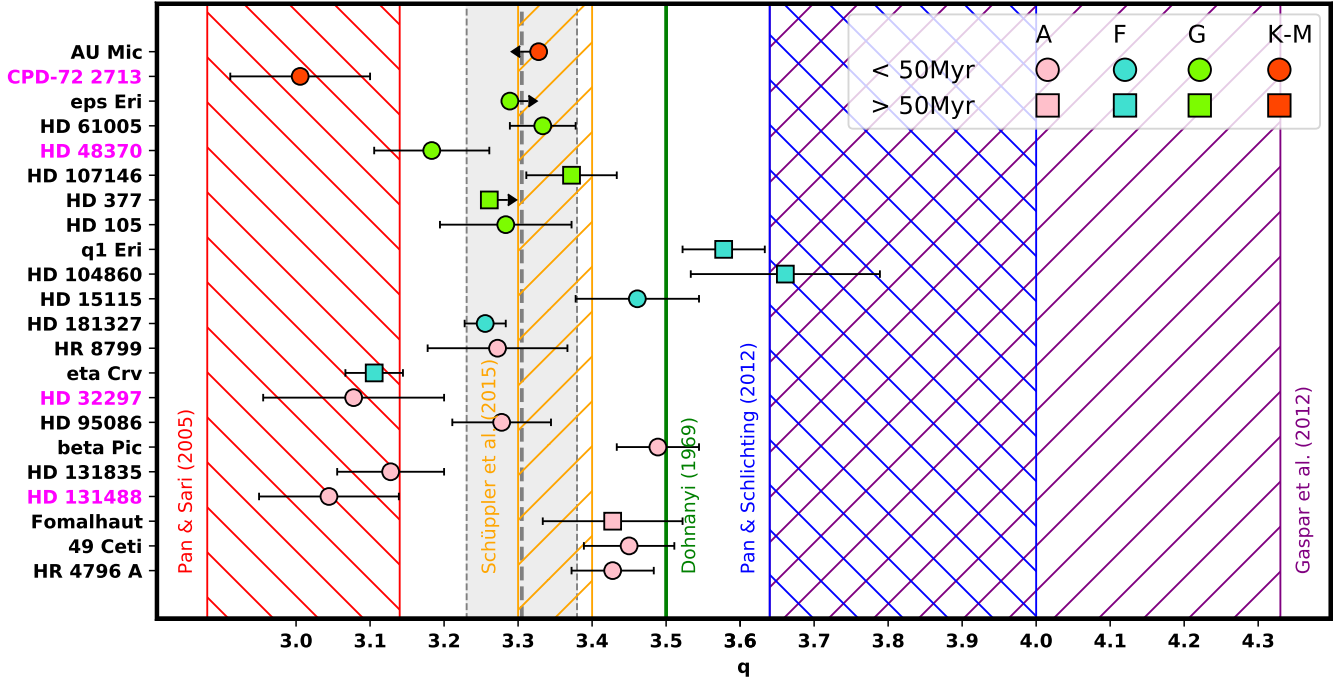


Figure 3. Distribution of grain size distribution power-law index q for the 22 debris disks. The labels for our four sources with new ATCA 8.8 mm flux are presented in magenta, while other sources are labelled in black as taken from [Löhne \(2020\)](#) (see references within). The mean weighted q value and associated uncertainty ($\langle q \rangle = 3.31 \pm 0.07$) is shown by the grey region. Sources are ordered by their stellar luminosity from top to bottom (see Table 3 for specific luminosity values). The solid lines and dashed regions indicate different model predictions: “rubble pile” planetesimals not dominated by material strength ([Pan & Sari \(2005\)](#); red), results of the ACE numerical model for AU Mic ([Schüppler et al. \(2015\)](#); yellow), the classic [Dohnányi \(1969\)](#) result (green), numerical results of [Gáspár et al. \(2012b\)](#) (purple), and incorporating a size-dependent velocity distribution ([Pan & Schlichting \(2012\)](#); blue). The markers are differentiated by spectral type and age (see Table A1 for values and references). For spectral types A, F, G, and K-M the markers have colours red, green, blue, and pink respectively. Targets with ages less than/greater than 50 Myr are represented by circle/square markers respectively.

of CO gas ($M_{\text{CO}} < 10^{-4} M_{\oplus}$, represented by open triangles in Figure 4), whereas 49 Ceti ([Moór et al. 2019](#)), HD 32297 ([Moór et al. 2019](#)), HD 131488 ([Moór et al. 2017](#)) and HD 131835 ([Moór et al. 2015](#)) are CO-rich ($M_{\text{CO}} > 0.01 M_{\oplus}$, represented by closed triangles in Figure 4). However we find no conclusive trend, although gas-rich systems have marginally lower q values than gas-poor disks. This could be the result of either a gas-rich debris system preventing blow out and retaining smaller grains via gas drag, or frequent grain collisions that give rise to excess gas as well as a cascade of small dust grains ([Lieman-Sifry et al. 2016](#)). After scaling the flux (Fig. 4b), it becomes apparent that there may exist two distributions of q in our sample. These include a broad distribution (for $q \sim 3.2-3.7$) of q for “typical” debris discs (gas-poor/non-detection) and a lower distribution (for $q < 3.2$) for bright gas-rich discs. To check this, we use a Fisher’s exact test on our data from Figure 4b (a Fisher’s test exactly calculates the significance of there existing two distinct distributions in a sample). We first separate the groups at $q=3.2$ and categorise the targets above and below 30 mJy (effectively separating our gas-rich discs and gas-poor/non-detection discs based on brightness), we obtain a significance of $p = 0.013$. If we instead categorise for gas-rich and gas-poor (which doesn’t take the brightness into account) we obtain a lower significance of $p = 0.04$. Thus, there is some evidence that bright (in absolute terms) gas-rich debris discs tend to contain lower q values (the first test with $p = 0.013$). Or alternately given that our systems are faint in apparent flux, it is possible that an observational bias exists, especially since the Pearson coefficient becomes weaker once we scale the flux with the distance. For a fixed FIR/mm flux (e.g. the DUNES survey, [Eiroa et al. 2013](#))

the discs with the steepest size distribution will result in \sim cm fluxes that are below the detection limit. It is quite plausible that there exist many discs lurking below current sensitivity levels ([Moro-Martín et al. 2015](#)) and, as a result, the current mean weighted q value would be biased towards lower values. If there indeed does exist a population of lower q discs then the mean weighted grain size power law index would shift closer towards the analytical models presented by [Pan & Sari \(2005\)](#) ($2.88 < q < 3.14$) where colliding bodies are held together by self-gravity and contain relatively low tensile strengths.

6 CONCLUSION

In this work we present new ATCA 8.8 mm observations of four debris discs and combine them to present the largest sample to date of 22 debris discs for which the grain size distribution power-law index q can be calculated to provide insights into the planetesimal populations in these discs. Our key findings are:

- (i) We present the longest wavelength observations to date of HD 48370, CPD-72 2713, HD 131488, and HD 32297 at 8.8 mm, and find that the q value of these sources are all quite low ($q < 3.2$), suggesting that the colliding bodies in these discs have a lower tensile strength and clumping is dominated by self-gravity.
- (ii) For the entire sample of 22 debris discs, we evaluate a weighted mean value of the sample, $\langle q \rangle = 3.31$, consistent with analytical and numerical predictions for collisional cascade models.

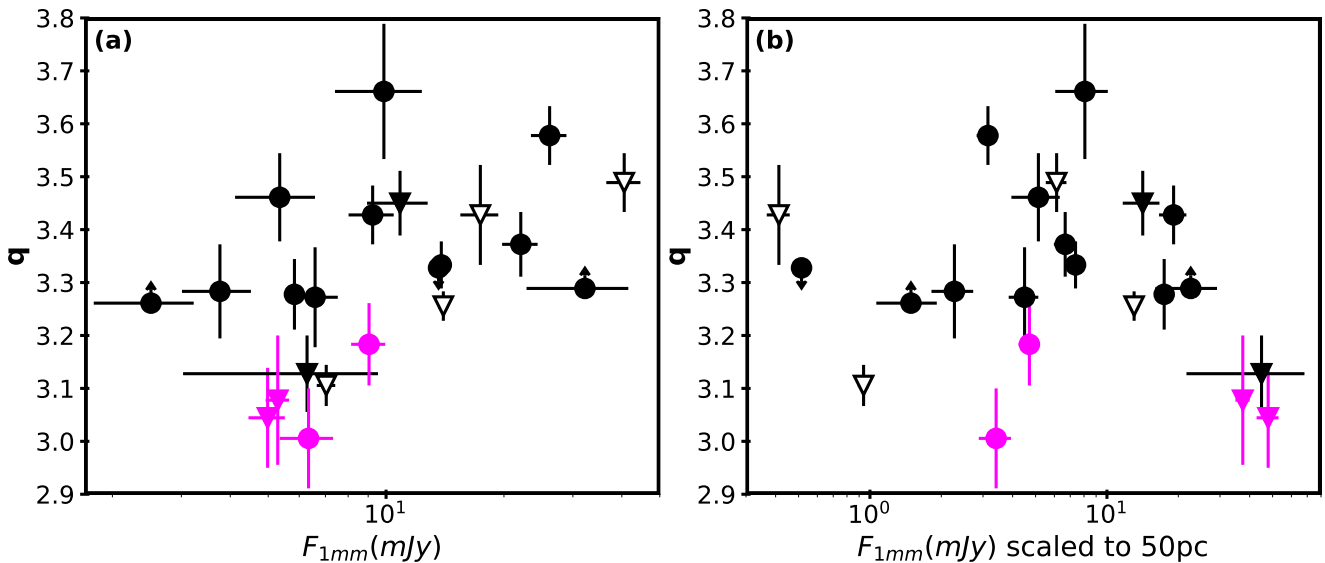


Figure 4. The grain size distribution parameter q as a function of (a) the interpolated 1 mm flux, and (b) the interpolated 1 mm flux scaled to a distance of 50 pc. Distances are taken from Gaia DR2 (Gaia Collaboration et al. 2018). Our four new ATCA 8.8 mm sources are labelled by magenta circles, and discs taken from the literature are labelled by black circles. Gas-rich sources are represented by closed triangles, and those that are gas-poor are represented by open triangles. The Pearson correlation for this relation for (a) is 0.57 and for (b) is -0.22.

(iii) With a larger sample (22 compared to 15 discs) we find that the tentative trend between q and the spectral type becomes weaker in comparison to findings from MacGregor et al. (2016).

(iv) We suggest possibility of two distributions of q ; a broad distribution (where $q \sim 3.2 - 3.7$) for "typical" debris discs (gas-poor/non-detection), and a lower distribution (where $q < 3.2$) for bright gas-rich discs.

(v) Or alternatively, we suggest an observational bias may be present between the grain size distribution parameter and absolute flux which is likely attributed to the detection rates of faint debris discs at \sim cm wavelengths.

ACKNOWLEDGEMENTS

The authors thank the referee for their constructive comments and suggestions. We thank Elodie Thilliez for useful discussions regarding our ATCA observing proposal. B.J.N. is supported by an Australian Government Research Training Program (RTP) Scholarship. G.M.K. is supported by the Royal Society as a Royal Society University Research Fellow. J.P.M. acknowledges research support by the Ministry of Science and Technology of Taiwan under grants MOST107-2119-M-001-031-MY3, MOST107-2119-M-001-031-MY3, and MOST109-2112-M-001-036-MY3, and Academia Sinica under grant AS-IA-106-M03. A.M. and P. Á. acknowledge support from the grant KH-130526 of the Hungarian NKFIH. The Australia Telescope Compact Array is part of the Australia Telescope which is funded by the Commonwealth of Australia for operation as a National Facility managed by CSIRO. This research has made use of NASA's Astrophysics Data System. The National Radio Astronomy Observatory is a facility of the National Science Foundation operated under agreement by the Associated Universities, Inc. ALMA is a partnership of ESO (representing its member states), NSF (USA) and NINS (Japan), together with NRC (Canada) and NSC and ASIAA (Taiwan) and KASI (Republic of Korea), in cooperation with the Republic of Chile. The Joint ALMA Observatory is operated by ESO, AUI/ NRAO

and NAOJ. This paper makes use of the following ALMA data: ADS/JAO.ALMA#2016.2.00200S

Software: The MIRIAD package (Sault et al. 1995), Python version 3.7, ASTROPY (Astropy Collaboration et al. 2013, 2018), SCI-PY (Virtanen et al. 2020), NUMPY (Harris et al. 2020), and MATPLOTLIB (Hunter 2007).

Facilities: Atacama Large Millimeter/sub-millimeter Array, Australian Telescope Compact Array

DATA AVAILABILITY

The ATCA observational data used in this paper is available from the Australian National Telescope Facility Archive at <https://atoa.atnf.csiro.au/> under project code C2696. The ALMA observational data is available from the ALMA science archive at <https://almascience.nrao.edu/aq/> under the project IDs listed in the Acknowledgements. Reduced observation data and models will be shared on reasonable request to the corresponding author.

REFERENCES

- Allard F., Homeier D., Freytag B., 2012, *From Interacting Binaries to Exoplanets: Essential Modeling Tools*, 282, 235
 Astropy Collaboration et al., 2013, *A&A*, 558, A33
 Astropy Collaboration et al., 2018, *AJ*, 156, 123
 Beckwith S. V. W., Sargent A. I., Chini R. S., Guesten R., 1990, *AJ*, 99, 924
 Bell C. P. M., Mamajek E. E., Naylor T., 2015, *MNRAS*, 454, 593
 Bohren C. F., Huffman D. R., 1983, Absorption and scattering of light by small particles
 Booth M., et al., 2017, *MNRAS*, 469, 3200
 Chen C. H., Sheehan P., Watson D. M., Manoj P., Najita J. R., 2009, *ApJ*, 701, 1367
 Choquet É., et al., 2016, *ApJ*, 817, L2
 Currie T., et al., 2012, *ApJ*, 757, 28
 Cutri R. M., et al., 2012, VizieR Online Data Catalog, p. II/281

- Debes J. H., Weinberger A. J., Kuchner M. J., 2009, *ApJ*, **702**, 318
- Dent W. R. F., et al., 2014, *Science*, **343**, 1490
- Dohnanyi J. S., 1969, *J. Geophys. Res.*, **74**, 2531
- Draine B. T., 2004, in *The Cold Universe*. p. 213 ([arXiv:astro-ph/0304488](https://arxiv.org/abs/astro-ph/0304488))
- Draine B. T., 2006, *ApJ*, **636**, 1114
- Duchêne G., et al., 2020, *AJ*, **159**, 251
- Eiroa C., et al., 2013, *A&A*, **555**, A11
- Esposito T. M., et al., 2020, *AJ*, **160**, 24
- Gagné J., et al., 2018, *ApJ*, **856**, 23
- Gaia Collaboration et al., 2016, *A&A*, **595**, A1
- Gaia Collaboration et al., 2018, *A&A*, **616**, A1
- Gaidos E., et al., 2014, *MNRAS*, **443**, 2561
- Gáspár A., Psaltis D., Ózel F., Rieke G. H., Cooney A., 2012a, *ApJ*, **749**, 14
- Gáspár A., Psaltis D., Rieke G. H., Ózel F., 2012b, *ApJ*, **754**, 74
- Gerbaldi M., Faraggiana R., Burnage R., Delmas F., Gómez A. E., Grenier S., 1999, *A&AS*, **137**, 273
- Greaves J. S., et al., 2016, *MNRAS*, **461**, 3910
- Harris C. R., et al., 2020, *Nature*, **585**, 357–362
- Holland W. S., et al., 2003, *ApJ*, **582**, 1141
- Holland W. S., et al., 2017, *MNRAS*, **470**, 3606
- Hughes A. M., et al., 2017, *ApJ*, **839**, 86
- Hughes A. M., Duchêne G., Matthews B. C., 2018, *ARA&A*, **56**, 541
- Hung L.-W., Fitzgerald M. P., Chen C. H., Mittal T., Kalas P. G., Graham J. R., 2015a, *ApJ*, **802**, 138
- Hung L.-W., et al., 2015b, *ApJ*, **815**, L14
- Hunter J. D., 2007, *Computing in Science & Engineering*, **9**, 90
- Jaeger C., Mutschke H., Begemann B., Dorschner J., Henning T., 1994, *A&A*, **292**, 641
- Kalas P., 2005, *ApJ*, **635**, L169
- Kennedy G. M., Wyatt M. C., 2014, *MNRAS*, **444**, 3164
- Kennedy G. M., Marino S., Matrà L., Panić O., Wilner D., Wyatt M. C., Yelverton B., 2018, *MNRAS*, **475**, 4924
- Kenyon S. J., Bromley B. C., 2002, *ApJ*, **577**, L35
- Kenyon S. J., Bromley B. C., 2008, *ApJS*, **179**, 451
- Kral Q., Marino S., Wyatt M. C., Kama M., Matrà L., 2019, *MNRAS*, **489**, 3670
- Krivov A. V., 2010, *Research in Astronomy and Astrophysics*, **10**, 383
- Krivov A. V., Booth M., 2018, *MNRAS*, **479**, 3300
- Lee J., Song I., 2018, *MNRAS*, **475**, 2955
- Liemman-Sifry J., Hughes A. M., Carpenter J. M., Gorti U., Hales A., Flaherty K. M., 2016, *ApJ*, **828**, 25
- Liseau R., et al., 2008, *A&A*, **480**, L47
- Liseau R., et al., 2010, *A&A*, **518**, L132
- Löhne T., 2020, *A&A*, **641**, A75
- Lommen D., et al., 2007, *A&A*, **462**, 211
- MacGregor M. A., et al., 2013, *ApJ*, **762**, L21
- MacGregor M. A., Wilner D. J., Andrews S. M., Hughes A. M., 2015a, *ApJ*, **801**, 59
- MacGregor M. A., Wilner D. J., Andrews S. M., Lestrade J.-F., Maddison S., 2015b, *ApJ*, **809**, 47
- MacGregor M. A., et al., 2016, *ApJ*, **823**, 79
- MacGregor M. A., et al., 2017, *ApJ*, **842**, 8
- MacGregor M. A., et al., 2018, *ApJ*, **869**, 75
- MacGregor M. A., et al., 2019, *ApJ*, **877**, L32
- Mamajek E. E., Meyer M. R., Liebert J., 2002, *AJ*, **124**, 1670
- Marino S., et al., 2016, *MNRAS*, **460**, 2933
- Marino S., et al., 2017, *MNRAS*, **465**, 2595
- Marino S., et al., 2018, *MNRAS*, **479**, 5423
- Marshall J. P., Maddison S. T., Thilliez E., Matthews B. C., Wilner D. J., Greaves J. S., Holland W. S., 2017, *MNRAS*, **468**, 2719
- Marshall J. P., Milli J., Choquet É., del Burgo C., Kennedy G. M., Matrà L., Ertel S., Boccaletti A., 2018, *ApJ*, **869**, 10
- Marshall J. P., Wang L., Kennedy G. M., Zeegers S. T., Scicluna P., 2021, *MNRAS*, **501**, 6168
- Matrà L., et al., 2017a, *MNRAS*, **464**, 1415
- Matrà L., et al., 2017b, *ApJ*, **842**, 9
- Matrà L., Wyatt M. C., Wilner D. J., Dent W. R. F., Marino S., Kennedy G. M., Milli J., 2019, *AJ*, **157**, 135
- Matthews B. C., Krivov A. V., Wyatt M. C., Bryden G., Eiroa C., 2014, in Beuther H., Klessen R. S., Dullemond C. P., Henning T., eds, *Protostars and Planets VI*. p. 521 ([arXiv:1401.0743](https://arxiv.org/abs/1401.0743)), [doi:10.2458/azu_uapress_9780816531240-ch023](https://doi.org/10.2458/azu_uapress_9780816531240-ch023)
- Matthews B. C., et al., 2015, *ApJ*, **811**, 100
- Melis C., Zuckerman B., Rhee J. H., Song I., Murphy S. J., Bessell M. S., 2013, *ApJ*, **778**, 12
- Moór A., et al., 2011, *ApJ*, **740**, L7
- Moór A., et al., 2015, *ApJ*, **814**, 42
- Moór A., Kóspál Á., Ábrahám P., Balog Z., Csengeri T., Henning T., Juhász A., Kiss C., 2016, *ApJ*, **826**, 123
- Moór A., et al., 2017, *ApJ*, **849**, 123
- Moór A., et al., 2019, *ApJ*, **884**, 108
- Moór A., et al., 2020, *AJ*, **159**, 288
- Moro-Martín A., et al., 2015, *ApJ*, **801**, 143
- Mustill A. J., Wyatt M. C., 2009, *MNRAS*, **399**, 1403
- Norfolk B. J., et al., 2021, *MNRAS*, **502**, 5779
- Pan M., Sari R., 2005, *Icarus*, **173**, 342
- Pan M., Schlichting H. E., 2012, *ApJ*, **747**, 113
- Paunzen E., 2015, *A&A*, **580**, A23
- Pawellek N., Krivov A. V., 2015, *MNRAS*, **454**, 3207
- Pawellek N., Krivov A. V., Marshall J. P., Montesinos B., Ábrahám P., Moór A., Bryden G., Eiroa C., 2014, *ApJ*, **792**, 65
- Pecaut M. J., Mamajek E. E., 2013, *ApJS*, **208**, 9
- Pecaut M. J., Mamajek E. E., Bubar E. J., 2012, *ApJ*, **746**, 154
- Ricarte A., Moldvai N., Hughes A. M., Duchêne G., Williams J. P., Andrews S. M., Wilner D. J., 2013, *ApJ*, **774**, 80
- Ricci L., Testi L., Maddison S. T., Wilner D. J., 2012, *A&A*, **539**, L6
- Ricci L., Carpenter J. M., Fu B., Hughes A. M., Corder S., Isella A., 2015a, *ApJ*, **798**, 124
- Ricci L., Maddison S. T., Wilner D., MacGregor M. A., Ubach C., Carpenter J. M., Testi L., 2015b, *ApJ*, **813**, 138
- Rizzuto A. C., Ireland M. J., Robertson J. G., 2011, *MNRAS*, **416**, 3108
- Sault R. J., Teuben P. J., Wright M. C. H., 1995, in Shaw R. A., Payne H. E., Hayes J. J. E., eds, *Astronomical Society of the Pacific Conference Series Vol. 77, Astronomical Data Analysis Software and Systems IV*. p. 433 ([arXiv:astro-ph/0612759](https://arxiv.org/abs/astro-ph/0612759))
- Schneider G., Silverstone M. D., Hines D. C., 2005, *ApJ*, **629**, L117
- Schüppler C., et al., 2015, *A&A*, **581**, A97
- Sibthorpe B., Kennedy G. M., Wyatt M. C., Lestrade J. F., Greaves J. S., Matthews B. C., Duchêne G., 2018, *MNRAS*, **475**, 3046
- Steele A., Hughes A. M., Carpenter J., Ricarte A., Andrews S. M., Wilner D. J., Chiang E., 2016, *ApJ*, **816**, 27
- Su K. Y. L., et al., 2017, *AJ*, **154**, 225
- Torres C. A. O., Quast G. R., da Silva L., de La Reza R., Melo C. H. F., Sterzik M., 2006, *A&A*, **460**, 695
- Torres C. A. O., Quast G. R., Melo C. H. F., Sterzik M. F., 2008, *Young Nearby Loose Associations*. p. 757
- Ubach C., Maddison S. T., Wright C. M., Wilner D. J., Lommen D. J. P., Koribalski B., 2012, *MNRAS*, **425**, 3137
- Ubach C., Maddison S. T., Wright C. M., Wilner D. J., Lommen D. J. P., Koribalski B., 2017, *MNRAS*, **466**, 4083
- Virtanen P., et al., 2020, *Nature Methods*, **17**, 261
- Williams J. P., Cieza L. A., 2011, *ARA&A*, **49**, 67
- Wilner D. J., MacGregor M. A., Andrews S. M., Hughes A. M., Matthews B., Su K., 2018, *ApJ*, **855**, 56
- Wilson W. E., et al., 2011, *MNRAS*, **416**, 832
- Wolf S., Voshchinnikov N. V., 2004, *Computer Physics Communications*, **162**, 113
- Wright E. L., et al., 2010, *AJ*, **140**, 1868
- Wyatt M. C., 2008, *ARA&A*, **46**, 339
- Wyatt M. C., Panić O., Kennedy G. M., Matrà L., 2015, *Ap&SS*, **357**, 103
- Yelverton B., Kennedy G. M., Su K. Y. L., Wyatt M. C., 2019, *MNRAS*, **488**, 3588
- Zuckerman B., Song I., 2012, *ApJ*, **758**, 77

**APPENDIX A: DEBRIS DISC SAMPLE
CHARACTERISTICS**

This paper has been typeset from a \TeX/L\AA\TeX file prepared by the author.

Table A1. Debris Disc Sample Characteristics. Targets are ordered identically to Table 3 and our four new PLATYPUS sources with ATCA 8.8 mm fluxes are in bold. r_d is the outer radial extent of the dust disc. $\lambda_{1,\text{mm}}$ and $\lambda_{2,\text{mm}}$ are the flux density values referenced in Table 3.

Source	SpT	Ref.	Age [Myr]	Ref.	r_d [au]	Ref.	Dist. ^a [pc]	$\lambda_{1,\text{mm}}$ [mJy]	Ref.	$\lambda_{2,\text{mm}}$ [μJy]	Ref.
AU Mic	M1	1	24	1	40	15	9.72	7.14 ± 0.15	34	$> 60.8 \pm 5.2$	1
CPD-72 2713	K-M	2	24	11	140	16	36.6	3.80 ± 0.59	16	95.9 ± 16.1	35
ϵ Eri	K2	1	400-800	1	69	17	41.8	17.2 ± 5.0	36	$66.1^{+6.9}_{-10.5}$	36
HD 61005	G8	1	40	1	67	18	36.4	7.2 ± 0.3	37	57.3 ± 8.6	1
HD 48370	G8	3	20-50	3	90	19	36.1	5.0 ± 0.5	35	70 ± 10.8	35
HD 107146	G2	1	80-200	1	116	20	27.4	12.5 ± 1.3	38	166.0 ± 25.2	39
HD 377	G2	1	150	1	101	21	38.5	3.5 ± 1.0	23	$< 13.1 \pm 4.4$	1
HD 105	G0	4	28	4	85	4	38.8	2.0 ± 0.4	4	42 ± 14	40
q^1 Eri	F9	1	4800	1	85	22	17.3	39.4 ± 4.1	41	92.6 ± 16.6	39
HD 104860	F8	1	140	1	110	23	45.2	4.4 ± 1.1	23	14.0 ± 3.5	1
HD 15115	F2	1	21	1	97	24	49.0	2.6 ± 0.6	42	12.8 ± 4.1	1
HD 181327	F6	1	24	1	86	25	48.2	7.5 ± 0.1	25	145.0 ± 19.2	39
HR 8799	A5	5	30	5	232	26	41.2	3.5 ± 0.5	26	32.6 ± 9.9	26
η Crv	F2	6	1000-2000	6	152	6	18.2	9.2 ± 0.5	6	< 36	40
HD 32297	A5/6	7	15-45	12	100	18	133	3.04 ± 0.21	12	56.2 ± 16.7	35
HD 95086	A8	1	17	1	208	27	86.4	3.1 ± 0.18	27	61.9 ± 15.9	39
β Pic	A6	1	24	1	106	28	19.4	60 ± 6	43	240.0 ± 33.2	39
HD 131835	A2	8	15	8	85	29	133	8.5 ± 4.4	44	53 ± 17	40
HD 131488	A2	9	15	14	91	30	155	2.91 ± 0.31	45	59.5 ± 12.4	35
Formalhaut	A4	1	440	1	136	31	7.70	27 ± 3	46	400 ± 64	47
49 Ceti	A1	1	40	1	95	32	57.1	17 ± 3	32	25.1 ± 5.5	1
HR 4796 A	A0	10	9	5	78	33	71.9	14.4 ± 1.9	5	< 63	40

Notes: ^a Distances are taken from Gaia Collaboration et al. (2018).

References (1) MacGregor et al. (2016), (2) Torres et al. (2006); Pecaut & Mamajek (2013), (3) Torres et al. (2008), (4) Marshall et al. (2018), (5) Holland et al. (2017), (6) Marino et al. (2017), (7) Debes et al. (2009), (8) Hung et al. (2015a), (9) Melis et al. (2013), (10) Gerbaldi et al. (1999), (11) Torres et al. (2006); Bell et al. (2015); Lee & Song (2018); Gagné et al. (2018), (12) MacGregor et al. (2018), (13) Mamajek et al. (2002); Pecaut et al. (2012), (15) Matthews et al. (2015), (16) Moór et al. (2020), (17) Booth et al. (2017), (18) MacGregor et al. (2018), (19) Moór et al. (2016), (20) Marino et al. (2018), (21) Choquet et al. (2016), (22) Liseau et al. (2010), (23) Steele et al. (2016), (24) MacGregor et al. (2019), (25) Marino et al. (2016), (26) Wilner et al. (2018), (27) Su et al. (2017), (28) Matrà et al. (2019), (29) Hung et al. (2015b), (30) Kral et al. (2019), (31) MacGregor et al. (2017), (32) Hughes et al. (2017), (33) Kennedy et al. (2018), (34) MacGregor et al. (2013) (35) this work, (36) MacGregor et al. (2015b), (37) Ricarte et al. (2013), (38) Ricci et al. (2015a), (39) Ricci et al. (2015b), (40) Marshall et al. (2017), (41) Liseau et al. (2008), (42) MacGregor et al. (2015a), (43) Dent et al. (2014), (44) Moór et al. (2015), (45) Moór et al. (2017), (46) Holland et al. (2003), (47) Ricci et al. (2012)